Mechanics Research Communications 87 (2018) 21–28

Contents lists available at ScienceDirect

Mechanics Research Communications

journal homepage: www.elsevier.com/locate/mechrescom

Oblique shear wave propagation in finitely deformed layered composites

Jian Li, Viacheslav Slesarenko, Pavel I. Galich, Stephan Rudykh*

Department of Aerospace Engineering, Technion – Israel Institute of Technology, Haifa 32000, Israel

ARTICLE INFO

Article history:
Received 21 August 2017
Received in revised form 5 December 2017
Accepted 5 December 2017
Available online 15 December 2017

Keywords:
Layered composite
Finite deformation
Wave propagation
Dispersion relation
Attenuation

ABSTRACT

In this paper, we study the influence of deformation on shear waves propagating at various angles in hyperelastic layered composites (LCs). In periodic laminates, shear wave band gaps (forbidden frequency ranges) exist only for waves propagating perpendicular to the layers, and the band gaps close suddenly if the incidence angle changes even slightly. However, the attenuation in the frequency ranges corresponding to band gap decreases gradually with a change in the angle. We find that the dispersion curves are significantly influenced by deformation for shear waves propagating at oblique angles. We show the evaluation of the dispersion from the case of waves propagating perpendicular to the layers to the case of waves propagating along the layers in finitely deformed LCs. We observe significant influence of deformation on the dispersion curves of shear waves propagating at angles different from the normal case. For waves propagating at angles close to the normal case, the dispersion curves are highly nonlinear, and the applied deformation changes the location of the local minima and maxima, and further transforms them. For oblique waves propagating at significantly different from normal case angles, we find that the dispersion curves possess "bi-linear" behavior, and the applied tensile deformation shifts the dispersion curves towards higher frequency in both linear short and long wave ranges. For long wave ranges, however, the effect of deformation becomes less significant after some level of applied deformation.

© 2017 Elsevier Ltd. All rights reserved.

1. Introduction

Elastic wave propagation in solids has been an active topic of research due to its importance for many applications, such as seismology, nondestructive testing, acoustic filters, vibration damper, biomedical imaging and acoustic cloaking. Recently, the field of architected microstructured metamaterials for manipulating elastic wave propagation has attracted significant attention [1–18]. Moreover, soft materials provide an opportunity to control elastic waves by deformation. This can be achieved through different effects of applied deformation – changes in microstructural geometry [19,20] and local material properties [21–25], or by a combination of these effects [26–28]. Furthermore, the influence of deformation can be further magnified by utilizing the elastic instability phenomenon. Buckling induced microstructure transformations can lead to formations of new periodic microstructures, thus, significantly influencing elastic wave propagation [29–32]. Experimental realization of such microstructured materials significantly depends on the development in material fabrications such as layer-by-layer fabricating and 3D printing techniques; these recently emerged techniques already allow manufacturing of microstructured materials at various length-scales [33–37].

Elastic wave propagation in finitely deformed homogeneous isotropic materials was pioneered by Biot [38], who investigated the influence of various cases of initial stress conditions on elastic wave propagations. Boulanger et al. [39] derived explicit expressions for phase velocities of shear and pressure waves propagation in compressible Hadamard materials. To account for the stiffening effects on elastic wave propagation, Galich et al. [22] studied the infinitesimal wave propagating in finitely deformed incompressible and compressible Gent materials and derived explicit expressions for phase velocities. Vinh and Merodio [40] investigated elastic wave propagation in incompressible transversely isotropic soft tissue. Vinh et al. [41] examined the influence of deformation and propagation direction on Rayleigh wave propagating in incompressible deformable transversely isotropic half-space; this study has been extended to the case of two family of fiber-reinforced elastic half-space by Nam et al. [42].

For the case of elastic waves propagating in layered composites (LCs), the pioneering work by Rytov [43] derived an explicit dispersion relation for steady state waves propagating perpendicular and parallel to the layers. In particular, for the case of waves propagating perpendicular to the layers, it was shown that the frequency spectrum consisted of an infinite number of modes with stop and pass

* Corresponding author.
E-mail address: rudykh@technion.ac.il (S. Rudykh).

https://doi.org/10.1016/j.mechrescom.2017.12.002
0093-6413/© 2017 Elsevier Ltd. All rights reserved.

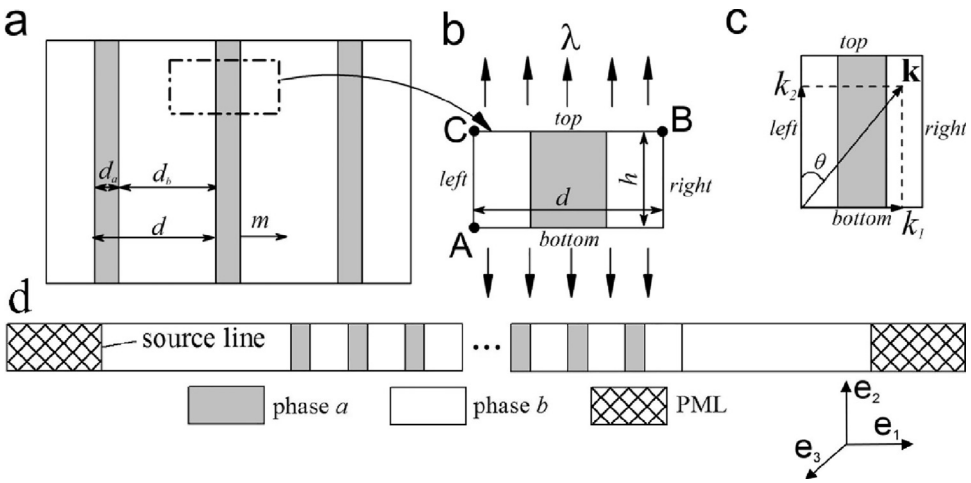

Fig. 1. Schematic of the unit cell and boundary conditions. (a) Periodic LCs with alternating phases *a* and *b*, (b) Unit cell with periodic boundary conditions, (c) Bloch wave boundary conditions superimposed on the deformed state, (d) Schematic of calculating transmittance coefficient of shear wave propagating in periodic LCs.

bands. Recently, Galich et al. [27] investigated the influence of large deformation on the elastic waves in deformable laminates. Galich et al. [27] obtained estimates for long shear waves propagating in any direction of the finitely deformed laminates with incompressible neo-Hookean phases. In addition to the long wave estimates, classical results of Rytov [43] have been extended to account for the effects of finite deformations, thus, allowing investigation of the influence of deformation on shear and pressure wave band gaps in laminates. Galich et al. [21] also showed that the shear wave band gaps in (incompressible and compressible) neo-Hookean LCs do not depend on deformation, as the deformation induced change in the geometry is fully compensated by the change in the effective material properties.

In this work, we focus on oblique shear waves propagating in finitely deformed LCs. We analyse the significant changes in the wave dispersion as the incidence angle starts to deviate from the normal case (wave propagation perpendicular to the layers) towards the oblique case. The most significant aspect is that the band gaps appear only for waves propagating perpendicular to the layers, and the band gaps do not appear if the propagation direction is changed even slightly. From the experimental point of view, it is extremely challenging to maintain the exact normal direction, so that the detection of the phenomenon may be affected by deviations in the actual propagation direction. While the band gaps close immediately, the transmission of the signal does not show a sudden change, but exhibit a gradual decrease with a change in the incidence angle from the normal direction. This was experimentally observed by Schneider et al. [44], who found strong attenuation in the band gap area of normal elastic wave propagation in LCs with alternating poly (methyl methacrylate) and porous silica; moreover, Schneider et al. [44] observed that the attenuation changed with a change in incidence angle. Here, we specifically focus on the influence of deformation on oblique shear wave propagation.

2. Numerical simulations

Let us consider periodic LCs consisted of two alternating nearly incompressible neo-Hookean phases with volume fraction $v_a = d_a/d$ and $v_b = 1 - v_a$ (as shown in Fig. 1(a)). Here and after, the quantities corresponding to phase *a* and phase *b* are denoted by subscripts $(\bullet)_a$ and $(\bullet)_b$, respectively. The constitutive behavior of each phase is defined through neo-Hookean strain energy function

$$W\left(\mathbf{F}_\xi\right) = \frac{\mu_\xi}{2}\left(\mathbf{F}_\xi : \mathbf{F}_\xi - 3\right) - \mu_\xi \ln\left(J_\xi\right) + \frac{\Lambda_\xi}{2}\left(J_\xi - 1\right)^2, \tag{1}$$

where Λ_ξ is the first Lame constant, μ_ξ is the shear modulus, $\mathbf{F}_\xi$ is the deformation gradient, and $J_\xi \equiv \det\left(\mathbf{F}_\xi\right)$, where ξ stands for *a* and *b*. To maintain a nearly incompressible behavior of the phases, we set a high ratio between the first Lame constant and shear modulus ($\Lambda_\xi/\mu_\xi = 10^4$). In this paper, we consider LCs in plane strain condition and apply macroscopic tensile deformation along the layers (as shown in Fig. 1(b)). The macroscopically applied deformation gradient is expressed as

$$\mathbf{F}_\xi = \lambda^{-1}\mathbf{e}_1 \otimes \mathbf{e}_1 + \lambda \mathbf{e}_2 \otimes \mathbf{e}_2 + \mathbf{e}_3 \otimes \mathbf{e}_3, \tag{2}$$

where, λ is the stretch ratio.

2.1. Bloch wave analysis

To obtain the dispersion relations for shear waves propagating in finitely deformed LCs, we employ the Bloch wave analysis implemented in the finite element based code COMSOL 5.2a. A unit cell, as shown in Fig. 1(b), is constructed for the simulations. The height of the unit cell, *h*, is set to be $0.1d$ to eliminate redundant eigenvalues and maintain reasonable computational time. The simulation procedures are performed in two steps: (**Step 1**) we apply an in-plane tension λ along the layer by the imposed periodic boundary conditions (Eq. (3)) to obtain the deformed state; (**Step 2**) we superimpose Bloch-Floquet periodic boundary conditions on the deformed unit cell (Eq. (4)). Then through solving the corresponding eigenvalue problems for a range of Bloch wave vectors [45–47], the dispersion relations for finitely deformed periodic LCs are obtained.

Step 1.

$$\begin{cases} u_1|_{right} = u_1|_{left} + u_1|_{\mathrm{B}} - u_1|_{\mathrm{C}} \\ u_2|_{right} = u_2|_{left} \\ u_1|_{top} = u_1|_{bottom} \\ u_2|_{top} = u_2|_{bottom} + (\lambda - 1)h \\ u_1|_{\mathrm{A}} = u_2|_{\mathrm{A}} = 0 \end{cases}, \tag{3}$$

where the index *right*, *left*, *top*, and *bottom* denote the sides of the unit cell. A, B and C correspond to the nodes at the corner of the unit cell (see Fig. 1(b)).

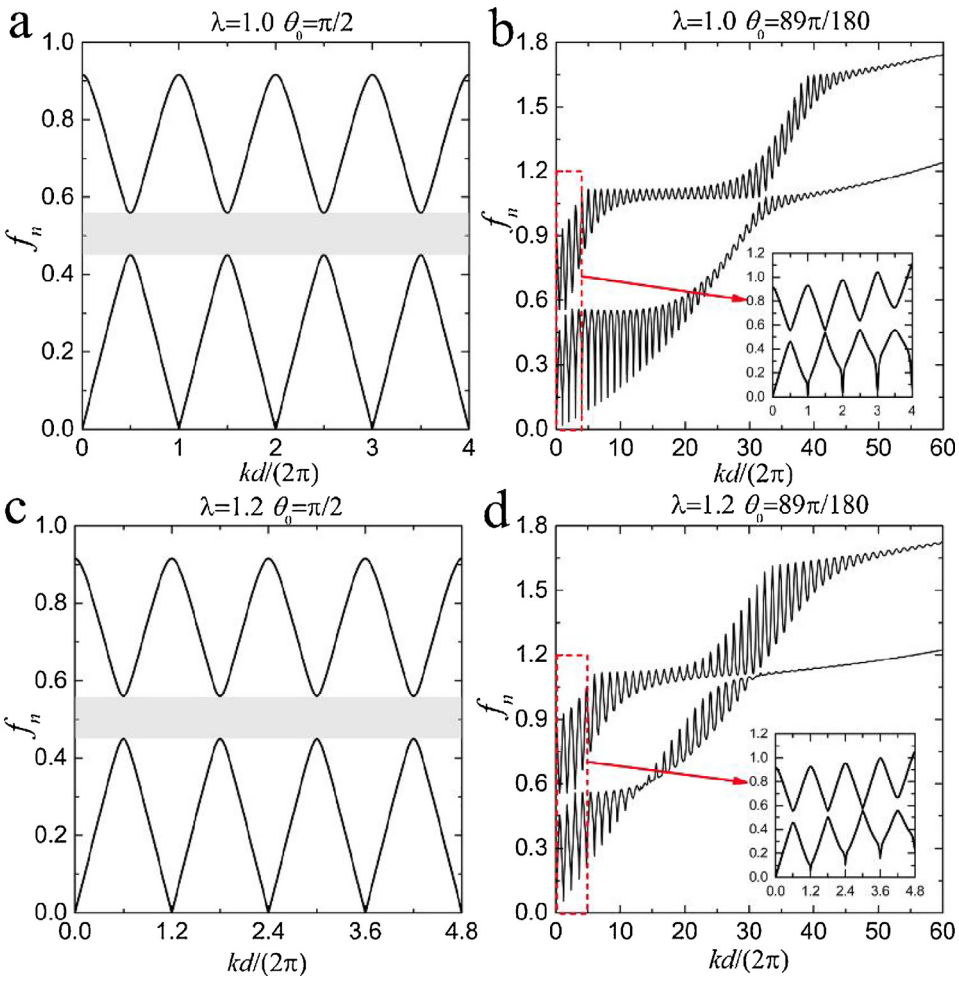

Fig. 2. Dispersion diagram of shear waves propagating in LCs ($\nu_a = 0.20$, $\mu_a/\mu_b = 100$, $\rho_a/\rho_b = 1$).

Step 2.

$$\begin{cases} u_1|_{right} = u_1|_{left} e^{-iK_1 d} \\ u_2|_{right} = u_2|_{left} e^{-iK_1 d} \\ u_1|_{top} = u_1|_{bottom} e^{-iK_2 h} \\ u_2|_{top} = u_2|_{bottom} e^{-iK_2 h} \end{cases}, \tag{4}$$

where K_1 and K_2 are the components of Bloch wave vector $\mathbf{K}$ in the undeformed configuration. Note that the Bloch wave vectors in the undeformed ($\mathbf{K} = |\mathbf{K}|\left(\sin\theta_0 \mathbf{e}_1 + \cos\theta_0 \mathbf{e}_2\right)$) and deformed configurations ($\mathbf{k} = |\mathbf{k}|\left(\sin\theta \mathbf{e}_1 + \cos\theta \mathbf{e}_2\right)$) are related, namely, $\mathbf{k} = \mathbf{F}^{-\mathrm{T}}\mathbf{K}$ [48]. Here, the angles θ_0 and θ define the directions of Bloch wave vectors in the undeformed and deformed configurations (see Fig. 1(c)), respectively. When the applied deformation takes the form of Eq. (2), the angles in the undeformed and deformed configurations are related as $\tan\theta = \lambda^2 \tan\theta_0$. Mesh sensitive analysis has been conducted to ensure that the relative error of the calculated frequency is less than 10^{-3}.

2.2. Transmittance spectra

To analyse the transmittance spectra of the waves propagating in the periodic LCs, the standard frequency domain analysis is performed. A schematic representation of the numerical model is shown in Fig. 1(d). An array of 32 unit cells is used in the numerical simulations. Two regions of homogenous matrix materials (4 times length of the period of the unit cell) are added to the left and right side of the LC. Perfectly matched layers (PMLs) are imposed on the two ends of the homogenous matrix regions to eliminate reflections. In addition, periodic boundary conditions are applied on the top and bottom boundaries. Finally, a harmonic vertical displacement with small amplitude is applied at the interface (denoted as the source line in Fig. 1(d)) between the left perfectly matched layer (PML) and the homogeneous material region. By measuring the amplitudes of the displacements in the left and right homogenous matrix areas denoted as u_{out} and u_{in}, respectively, we obtain the transmittance coefficient defined as $\varphi = 10\lg(u_{out}/u_{in})$.

3. Results and discussions

We start from consideration of the influence of small deviation in the wave propagation direction from the normal case (waves propagating perpendicular to the layers) on the dispersion relations. First, we compare the dispersion relations of shear waves propagating in undeformed and deformed LCs in the direction (a) perpendicular to the layers ($\theta_0 = \pi/2$) and (b) with a small deviation from the normal direction ($\theta_0 = 89\pi/180$). Here frequency is normalized as $f_n = \omega d\sqrt{\tilde{\rho}/\tilde{\mu}}/(2\pi)$, where ω is the angular frequency, $\tilde{\rho} = \nu_a\rho_a + \nu_b\rho_b$ is the average density, and $\tilde{\mu} = \left(\nu_a/\mu_a + \nu_b/\mu_a\right)^{-1}$. In perfect agreement with the theoretical results [27,43], the dispesion structure for the normal case is periodic and possesses band gaps (denoted by the shaded grey areas in Fig. 2(a) and (c)). The first shear wave band gap (BG) is located in the range of the normalized frequency from 0.45 to 0.55 and it is not

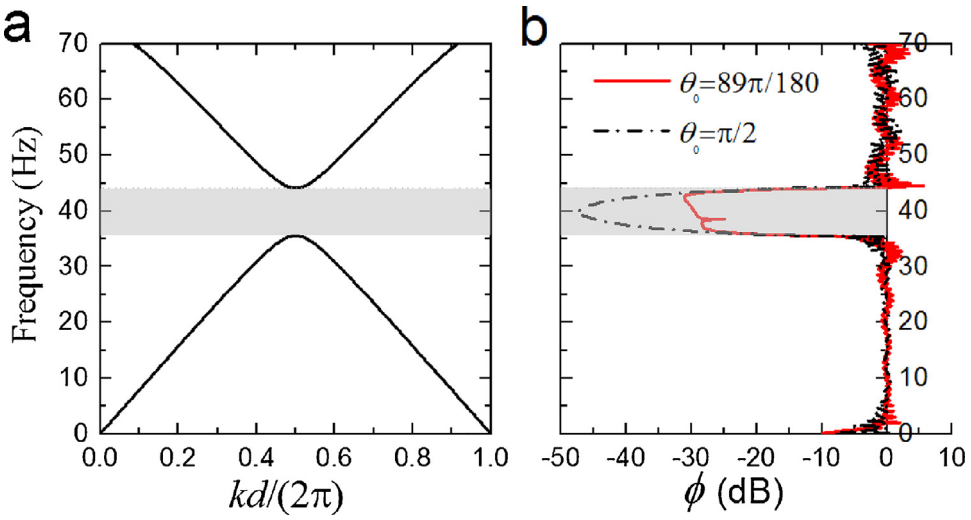

Fig. 3. Band gaps and transmittance spectra for LC with $d = 1$m, $v_a = 0.20$, $\mu_a = 500$MPa, $\mu_b = 5$MPa, $\rho_a = \rho_b = 10^3$kg/m^3. (a) Band gaps of shear waves propagating perpendicular to the layers, (b) Transmittance spectra for shear waves propagating perpendicular to the layers ($\theta_0 = \pi/2$ – dash-dotted black curve) and at a slightly oblique angle ($\theta_0 = 89\pi/180$ – continuous red curve).

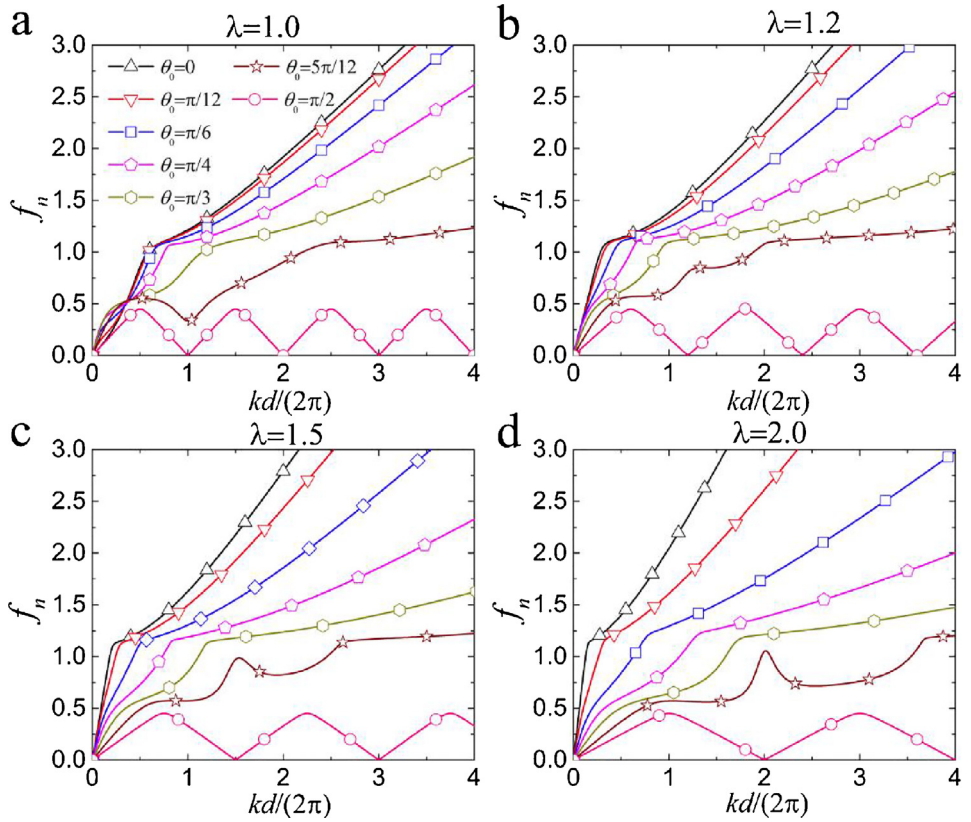

Fig. 4. Dispersion curves for oblique shear waves propagating in LCs ($v_a = 0.20$, $\mu_a/\mu_b = 100$, $\rho_a/\rho_b = 1$) subjected to different deformation levels.

affected by deformation (see Fig. 2(a) and (c)). This is in full agreement with the results by Galich et al. [27] that showed that the BGs for shear waves propagating perpendicular to neo-Hookean layers were independent of the applied deformation. However, when the direction of propagation is changed even slightly, for example, $\theta_0 = 89\pi/180$, we observe the absence of BGs (see Fig. 2 (b) for the undeformed state and Fig. 2 (d) for the deformed state). We note that for relatively small normalized wavenumbers (see the range from 0 to 4 in Fig. 2(b) and (d)), the dispersion curves for $\theta_0 = 89\pi/180$ are somewhat similar to the normal case. We also observe the peak frequencies of the lower branch increase with an increase in wavenumber (see Fig. 2(b) and (d)), leading to the absence of the BGs as opposite to the normal case (see Fig. 2(a) and (c)). Thus, the BGs of the undeformed and deformed LCs disappear immediately once the direction of wave propagation is changed from the perpendicular direction.

Next, we illustrate the attenuation characteristics for shear wave propagation in LCs for two cases: (a) normal case, (b) a small deviation from the normal case. The dispersion curves for shear waves propagating perpendicular to the layers are plotted in Fig. 3(a), the transmittance spectra for different incidence angles are plotted in Fig. 3(b). In the calculation of transmittance spectra of the LCs, the

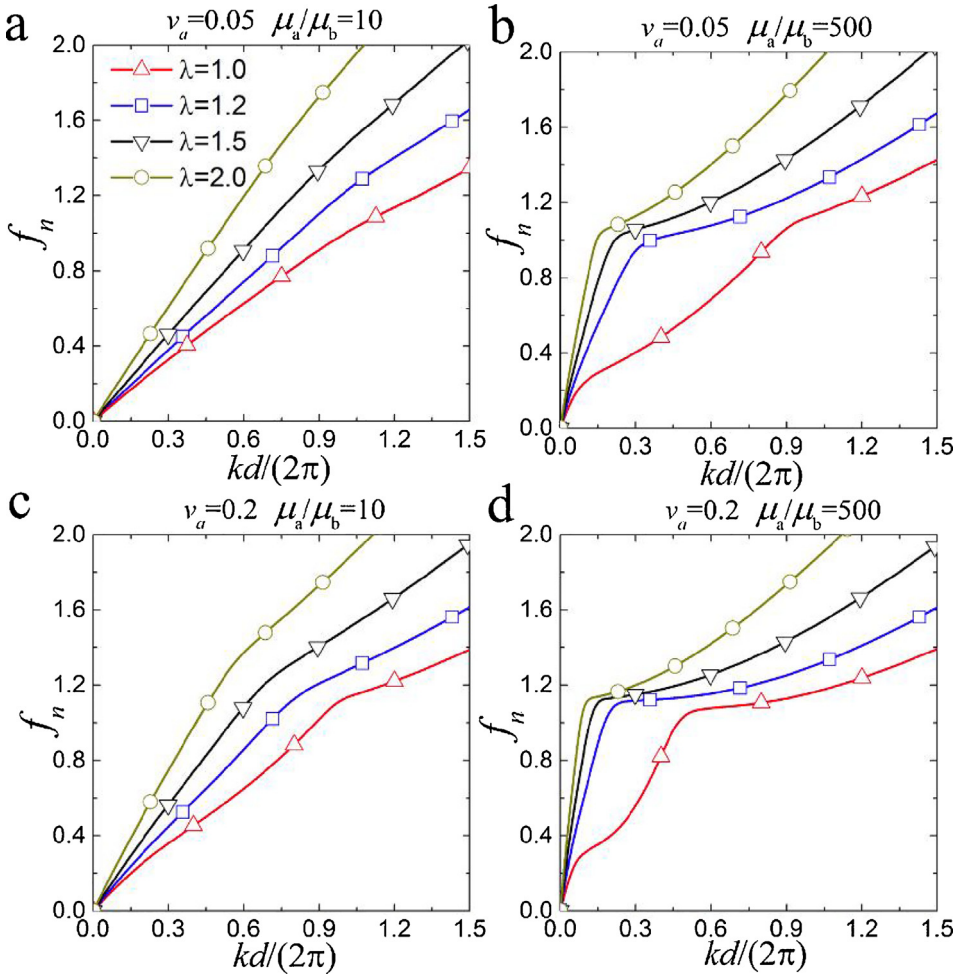

Fig. 5. Dispersion curves for oblique shear waves propagating at $\theta = \pi/6$ in LCs with $\rho_a/\rho_b = 1$ and (a)$v_a = 0.05$, $\mu_a/\mu_b = 10$; (b)$v_a = 0.05$, $\mu_a/\mu_b = 500$; (c)$v_a = 0.20$, $\mu_a/\mu_b = 10$; (d)$v_a = 0.20$, $\mu_a/\mu_b = 500$.

following geometrical and material parameters are used: $d = 1$ m, $v_a = 0.20$, $\mu_a = 500$MPa, $\mu_b = 5$MPa, $\rho_a = \rho_b = 10^3$kg/m^3. The continuous red curve corresponds to the case of $\theta_0 = 89\pi/180$, and the dash-dotted black curve is for the case of $\theta_0 = \pi/2$. When waves propagate perpendicular to the layers ($\theta_0 = \pi/2$), strong attenuations is observed in the frequency range of the band gap. Again, for the case with a slightly deviation ($\theta_0 = 89\pi/180$), there is no band gap; however, the corresponding attenuations (in the band gap area of $\theta_0 = \pi/2$) are still significant, although it is reduced as compared to the normal case. Thus, the band gaps disappear immediately with a change in the incidence angle, but the transmittance characteristics change (decrease) gradually.

To clarify how the dispersion curves of shear wave propagation in LCs transform from perpendicular to parallel to the layer direction, we present the dispersion curves for various directions of shear wave propagation in Fig. 4. We note that the dispersion curves are in good agreement with the long wave estimates [27]. Examples of comparisons between the long wave estimates and the Bloch wave numerical results are shown in the Appendix A. Fig. 4 shows that the dispersion curves gradually change from $\theta_0 = \pi/2$ to $\theta_0 = 0$ for the undeformed (a) and finitely stretched (λ = 1.2 (b), λ = 1.5 (c), and λ = 2.0 (d)) laminates. We note that in accordance with the previous results, the periodicity of the dispersion curves breaks once the incidence angle change from $\theta_0 = \pi/2$. We observe that for oblique cases the dispersion curves are characterized by the existence of two typical linear ranges (in the long wave range and in the short wave range). However, for the cases that are close to the normal case ($\theta_0 = \pi/2$), the transition range between these two linear regimes is characterized by significant nonlinearities (see, for example, the dispersion curves corresponding to $\theta_0 = 5\pi/12$ in Fig. 4). Remarkably, the dispersion curves are significantly influenced by deformation (compare the corresponding curves in Fig. 4(a) and (c)). For example, for $\theta_0 = 5\pi/12$, in the undeformed state, there is a prominent local minimum at $kd/2\pi \approx 1$; however, application of deformation of λ = 1.5 eliminates this local minimum. Also, for smaller angles, such as $\theta_0 \leq \pi/3$, we clearly find the applied tensile deformation in the direction of the layers leads to a sharper transition between these two linear regimes.

Fig. 5 shows the examples of influence of deformation on the dispersion curves for shear waves propagating at $\theta = \pi/6$ in LCs with various volume fractions and stiffness ratio of the phases. In agreement with our previus results, we also observe that the dispersion curves have two typical linear ranges, and the nonlinearities of the transition range between these two linear regimes increase with an increasing role of stiffer layers (higher shear modulus contrast and/or volume fraction of the stiffer layer). Meanwhile, the tensile deformation shifts the dispersion curves towards higher frequencies. For example, the LC with $v_a = 0.05$ and $\mu_a/\mu_b = 10$, the applied deformation of λ = 1.5 shifts the frequency (at $kd/2\pi = 1.0$) from $f_n = 0.99$ (in the undeformed LC) up to 1.47. Moreover, we observe that for longer waves the influence of deformation becomes less pronounced after certain deformation level (which depends on the material composition). For example, for LC with $v_a = 0.2$, $\mu_a/\mu_b = 500$, the applied deformation of λ = 1.5 shifts

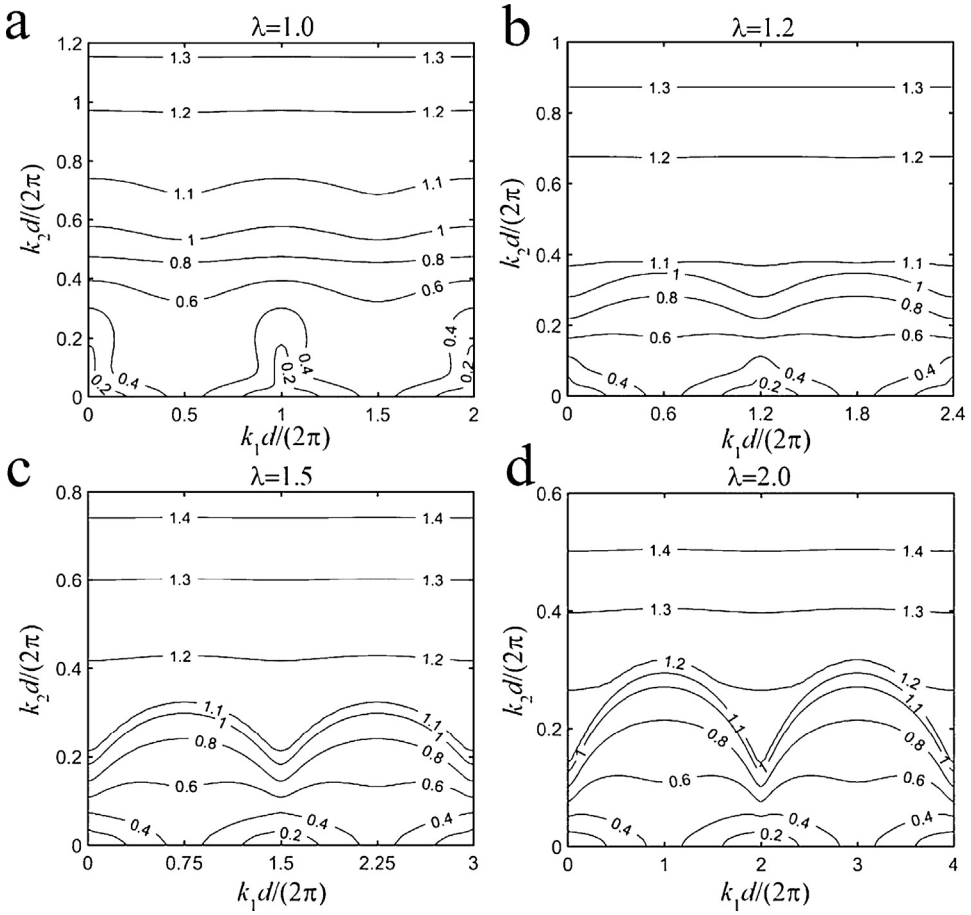

Fig. 6. Equifrequency curves of shear waves propagating in undeformed (a) and deformed (b, c and d) LCs ($\nu_a = 0.20$, $\mu_a/\mu_b = 100$, $\rho_a/\rho_b = 1$).

the frequency (at $kd/2\pi = 0.3$) from $f_n = 0.56$ (in the undeformed LC) up to 1.15; whereas the frequency increases only up to 1.20 with further increase of deformation up to $\lambda = 2.0$. The corresponding deformation level (after which the influence of deformation becomes less pronounced) is lower for LCs with more significant role of the stiffer layers (compare Fig. 5(a) and (d)).

To provide more details on the oblique shear waves, we plot the equifrequency curves in Fig. 6. Due to the periodic laminate structure, the equifrequency curves are periodic in the direction of k_1, and are not periodic in the direction of k_2. Specially, for the equifrequency curves of undeformed LC in a period ($0 \le k_1 d/(2\pi) \le 1$), we find that the maximum and minimum frequencies at a certain k_2 are always located at $k_1 d/(2\pi) = 0.5$ and $k_1 d/(2\pi) = 0$, respectively (see Fig. 6(a)). However, an increase in k_2, leads to the situation when the equifrequncy curves become smooth, and the prominent minima/maxima points disappear. Furthermore, applied deformation leads to a change in the periodicity due to the change in the layer thicknesses, namely, the period of k_1 changes from $\Delta k_1 d/(2\pi) = 1$ (in the undeformed state) to $\Delta k_1 d/(2\pi) = 1.5$ for the laminates stretched to $\lambda = 1.5$ level (see Fig. 6(c)). The applied deformation significantly influences the shape of the equifrequency curves. For example, compared with the contour lines at $f_n = 0.4, 0.6, 0.8$ in the undeformed state (see Fig. 6(a)), we observe maximum frequency for a certain k_2 gradually changes from $k_1 d/(2\pi) = 0.5$ to $k_1 d/(2\pi) = 0$ in the deformed state (see Fig. 6(c)). In addition, the deformation also shifts the equifrequency curves towards higher frequencies. For instance, the curves corresponding to $f_n = 1.2$ in the undeformed and deformed ($\lambda = 2.0$) states are located at $k_2 d/(2\pi) \approx 0.97$ and 0.30, respectively.

4. Conclusion

We have studied shear waves propagating in finitely deformed LCs with nearly incompressible neo-Hookean phases. By application of Bloch wave analysis superimposed on large deformation, we obtained the dispersion curves for shear waves propagating at normal and oblique angles relative to the layers. We have found that the band gaps close immediately when the direction of wave propagation changes even slightly from the normal propagation direction – this is for both undeformed and deformed laminates. The attenuation, however, decreases gradually with a change in the direction of wave propagation. We have observed that the dispersion curves of shear waves propagating in LCs change suddenly when the direction of propagation changes (even slightly) from perpendicular to the layer direction. Further change in the propagation direction leads to a graduate change in the dispersion curves. For small deviation angles (from the normal case), the dispersion curves exhibit significant nonlinearities; and prominent picks are observed. These picks evolve with the further change in the angle, and, at certain oblique propagation direction, the dispersion curves are characterized by two linear ranges. The transition wavenumber between these two linear regimes depends on the LC composition, and the corresponding transition wavenumber is observed to increase with an increasing role of stiffer layers (higher shear modulus contrast and larger volume fraction of the stiffer layer).

The dispersion curves for the oblique waves are found to be significantly affected by the applied deformation. In particular, the highly nonlinear behavior of dispersion curves (for waves propagating at the angles close to the normal case), is significantly transformed through the applied deformation. More specifically,

the local minima can be significantly smoothen and even transformed into local maxima by increasing the applied deformation level. Furthermore, for oblique waves propagating at large angles (relative to the normal case) corresponding to the "bi-linear" regime, we have observed that the increased tensile deformation shifted the dispersion curves towards higher frequencies. This is valid for both linear ranges (short and long wave ranges) of the oblique waves. For longer waves, however, the influence of deformation becomes less pronounced after certain deformation level, which is defined by LC composition (the deformation level is lower for LCs with more significant role of the stiffer layers).

Acknowledgements

This work was supported by the Israel Science Foundation (grant No. 1550/15 and 1973/15). SR gratefully acknowledges the support of Taub Foundation through the Horev Fellowship-Leaders in Science and Technology. JL thanks the support of Lady Davis graduate student fellowship. PG acknowledges the support of Jacobs Fellowship. VS thanks the Technion postdoctoral fellowship.

Appendix A. Comparisons of long wave estimates and Bloch wave numerical analyses

The long wave estimates of shear waves propagating in LCs subjected to any homogeneous deformation can be expressed as

$$\omega = \sqrt{b/\bar{\rho}}, \tag{A. 1}$$

where

$$b = \bar{\mu}\left(\mathbf{k}\cdot\bar{\mathbf{B}}\cdot\mathbf{k}\right) + (\tilde{\mu}-\bar{\mu})\left(\mathbf{k}\cdot\bar{\mathbf{F}}\cdot\mathbf{m}\right)^2 + \frac{\bar{\mu}-\tilde{\mu}}{\alpha^2}\left(\frac{4\beta_k^2}{\alpha}-k^2\right)\left(\alpha-\frac{\beta_k^2}{k^2}\right) \tag{A.2}$$

where $\mathbf{k}$ is the wave vector,$k = |\mathbf{k}|$ is the wavenumber,$\bar{\mathbf{F}} = \upsilon_a\mathbf{F}_a + \upsilon_b\mathbf{F}_b$ is the average deformation gradient; $\bar{\mathbf{B}} = \bar{\mathbf{F}}\cdot\bar{\mathbf{F}}^{\mathrm{T}}$ is the average left Cauchy-Green deformation tensor; $\mathbf{m}$ is the direction of LCs (see Fig. 1(a)); $\alpha = \mathbf{m}\cdot\bar{\mathbf{C}}^{-1}\cdot\mathbf{m}$, $\beta_k = \mathbf{k}\cdot\bar{\mathbf{F}}^{\mathrm{T}}\cdot\mathbf{m}$, $\bar{\mu} = \nu_a\mu_a + \nu_b\mu_b$.

Here we show the comparison of the analytical long wave estimates and Bloch wave numerical results for shear waves propagating in LCs in the direction of Bloch wave vector $\theta_0 = \pi/12$. The examples are given for LCs subjected to a deformation of $\lambda = 1.5$. Fig. A1(a) and (b) show the comparisons for LCs with $\nu_a = 0.20$, $\mu_a/\mu_b = 10$ and $\mu_a/\mu_b = 500$, respectively; Fig. A1(c) and (d) show the results for $\nu_a = 0.05$, $\mu_a/\mu_b = 10$ and $\mu_a/\mu_b = 500$, respectively. Here we consider LCs with the phases characterized by identical densities. The continuous black curves represent the Bloch wave numerical results, and the dash-dotted red curves correspond to the long wave estimates. For LCs with small volume fractions and shear modulus

contrasts, such as shown in Fig. A1(c), $\nu_a = 0.05$, $\mu_a/\mu_b = 10$, the long wave estimate is in good agreement with the result of simulation up to the wavelengths comparable to the period of LC. However, with an increase in volume fraction and shear modulus contrast, the difference increases. For instance, for LCs with $\mu_a/\mu_b = 10$, $\nu_a = 0.05$ and $\nu_a = 0.20$, the long wave estimate curves and Bloch wave numerical curves start to differ after wavenum-

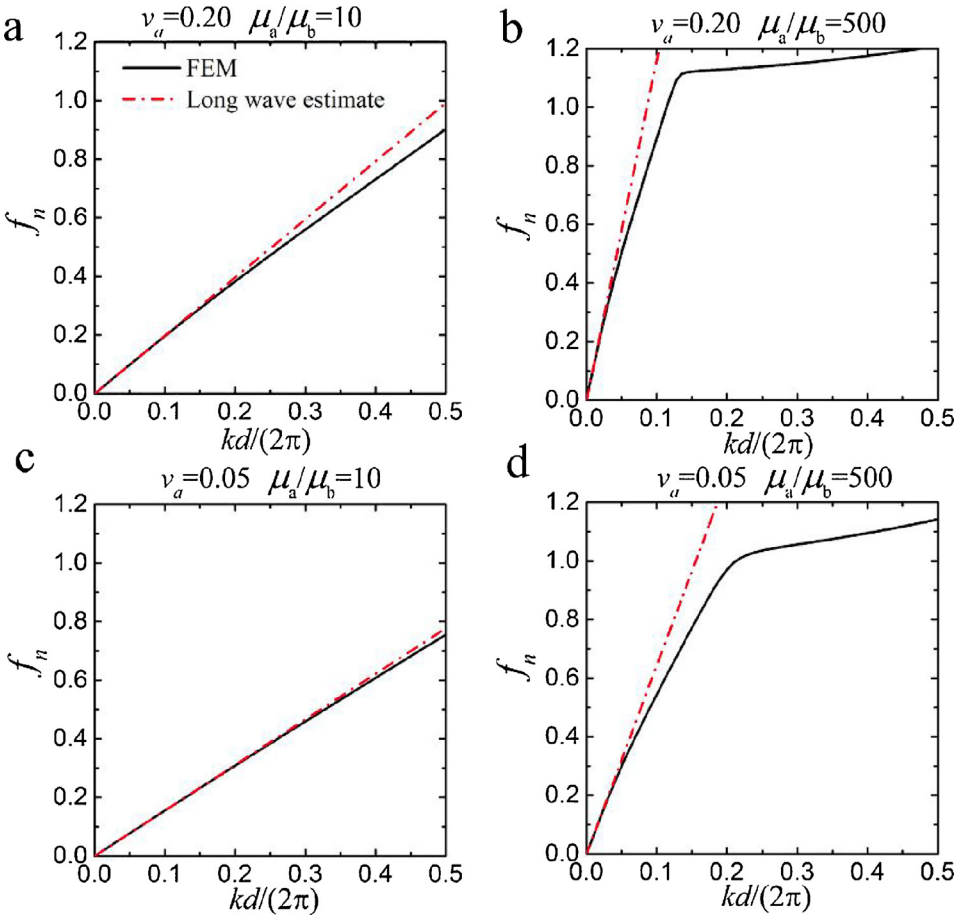

Fig. A1. Comparisons of long wave estimates and numerical analyses for shear waves propagating in LCs with $\theta_0 = \pi/12$. LCs are considered as $\rho_a/\rho_b = 1$ and (a)$\nu_a = 0.20$, $\mu_a/\mu_b = 10$ (b)$\nu_a = 0.20$, $\mu_a/\mu_b = 500$ (c)$\nu_a = 0.05$, $\mu_a/\mu_b = 10$ (d)$\nu_a = 0.05$, $\mu_a/\mu_b = 500$. The LCs are subjected to a tension of $\lambda = 1.5$.

ber $kd/(2\pi) \approx 0.4$ and 0.2, respectively. For LCs with $\mu_a/\mu_b = 1000$, the significantly differences are observed after the wavenumber $kd/(2\pi) \approx 0.05$ ($\nu_a = 0.05$) and 0.03 ($\nu_a = 0.20$), respectively. Thus, the difference of long wave estimates increases with an increase in volume fraction and shear modulus contrast. This observation is similar to the one for three dimensional hyperelastic fiber composites [47].

References

[1] S. Babaee, N. Viard, P. Wang, N.X. Fang, K. Bertoldi, Harnessing deformation to switch on and off the propagation of sound, Adv. Mater. 28 (2016) 1631–1635.
[2] D. Bigoni, S. Guenneau, A.B. Movchan, M. Brun, Elastic metamaterials with inertial locally resonant structures: application to lensing and localization, Phys. Rev. B 87 (2013) 174303.
[3] P. Celli, S. Gonella, Manipulating waves with LEGO® bricks: a versatile experimental platform for rmetamaterial architectures, Appl. Phys. Lett. 107 (2015), 081901.
[4] Y. Chen, L. Wang, Bio-inspired heterogeneous composites for broadband vibration mitigation, Sci. Rep. 5 (2016) 17865.
[5] F. Javid, P. Wang, A. Shanian, K. Bertoldi, Architected materials with ultra-low porosity for vibration control, Adv. Mater. 28 (2016) 5943–5948.
[6] M. Miniaci, A. Krushynska, A.B. Movchan, F. Bosia, N.M. Pugno, Spider web-inspired acoustic metamaterials, Appl. Phys. Lett. 109 (2016), 071905.
[7] K.H. Matlack, A. Bauhofer, S. Krödel, A. Palermo, C. Daraio, Composite 3D-printed metastructures for low-frequency and broadband vibration absorption, Proc. Natl. Acad. Sci. 113 (2016) 8386–8390.
[8] G. Trainiti, J.J. Rimoli, M. Ruzzene, Wave propagation in undulated structural lattices, Int. J. Solids Struct. 97–98 (2016) 431–444.
[9] J. Meaud, K. Che, Tuning elastic wave propagation in multistable architected materials, Int. J. Solids Struct. 122–123 (2017) 69–80.
[10] J. Xu, X. Jiang, N. Fang, E. Georget, R. Abdeddaim, J.M. Geffrin, M. Farhat, P. Sabouroux, S. Enoch, S. Guenneau, Molding acoustic, electromagnetic and water waves with a single cloak, Sci. Rep. 5 (2015) 10678.
[11] S. Zhang, C. Xia, N. Fang, Broadband acoustic cloak for ultrasound waves, Phys. Rev. Lett. 106 (2011), 024301.
[12] R. Zhu, X.N. Liu, G.K. Hu, C.T. Sun, G.L. Huang, Negative refraction of elastic waves at the deep-subwavelength scale in a single-phase metamaterial, Nat. Commun. 5 (2014) 5510.
[13] L. Zigoneanu, B.I. Popa, S.A. Cummer, Three-dimensional broadband omnidirectional acoustic ground cloak, Nat. Mater. 13 (2014) 352–355.
[14] A. Srivastava, Metamaterial properties of periodic laminates, J. Mech. Phys. Solids 96 (2016) 252–263.
[15] P. Zhang, W.J. Parnell, Band gap formation and tunability in stretchable serpentine interconnects, J. Appl. Mech. 84 (2017), 091007.
[16] M.A. Jandron, D. Henann, Exploring phononic crystal tunability using dielectric elastomers, J. Acoust. Soc. Am. 141 (2017) 3743.
[17] P. Celli, S. Gonella, V. Tajeddini, A. Muliana, S. Ahmed, Z. Ounaies, Wave control through soft microstructural curling: bandgap shifting, reconfigurable anisotropy and switchable chirality, Smart Mater. Struct. 26 (2017), 035001.
[18] P.I. Galich, S. Rudykh, Shear wave propagation and band gaps in finitely deformed dielectric elastomer laminates: long wave estimates and exact solution, J. Appl. Mech. 84 (2017), 091002.
[19] P. Wang, J. Shim, K. Bertoldi, Effects of geometric and material nonlinearities on tunable band gaps and low-frequency directionality of phononic crystals, Phys. Rev. B. 88 (2013), 014304.
[20] F. dell'Isola, I. Giorgio, M. Pawlikowski, N.L. Rizzi, Large deformations of planar extensible beams and pantographic lattices: heuristic homogenization, experimental and numerical examples of equilibrium, Proc. R. Soc. A Math. Phys. Eng. Sci. 472 (2016) 20150790.
[21] Z. Chang, H.Y. Guo, B. Li, X.Q. Feng, Disentangling longitudinal and shear elastic waves by neo-Hookean soft devices, Appl. Phys. Lett. 106 (2015) 161903.
[22] P.I. Galich, S. Rudykh, Influence of stiffening on elastic wave propagation in extremely deformed soft matter: from nearly incompressible to auxetic materials, Extrem. Mech. Lett. 4 (2015) 156–161.
[23] P.I. Galich, S. Rudykh, Manipulating pressure and shear waves in dielectric elastomers via external electric stimuli, Int. J. Solids Struct. 91 (2016) 18–25.
[24] M. Destrade, R.W. Ogden, On stress-dependent elastic moduli and wave speeds, IMA J. Appl. Math. 78 (2013) 965–997.
[25] P.I. Galich, S. Rudykh, Comment on Disentangling longitudinal and shear elastic waves by neo-Hookean soft devices [Appl. Phys. Lett. 106, 161903 (2015)], Appl. Phys. Lett. 107 (2015), 056101.
[26] Q. Chen, A. Elbanna, Modulating elastic band gap structure in layered soft composites using sacrificial interfaces, J. Appl. Mech. 83 (2016) 111009.
[27] P.I. Galich, N.X. Fang, M.C. Boyce, S. Rudykh, Elastic wave propagation in finitely deformed layered materials, J. Mech. Phys. Solids 98 (2017) 390–410.
[28] N.T. Nam, J. Merodio, R.W. Ogden, P.C. Vinh, The effect of initial stress on the propagation of surface waves in a layered half-space, Int. J. Solids Struct. 88–89 (88) (2016) 88–100.
[29] S. Rudykh, M.C. Boyce, Transforming wave propagation in layered media via instability-induced interfacial wrinkling, Phys. Rev. Lett. 112 (2014), 034301.
[30] S. Shan, S.H. Kang, P. Wang, C. Qu, S. Shian, E.R. Chen, K. Bertoldi, Harnessing multiple folding mechanisms in soft periodic structures for tunable control of elastic waves, Adv. Funct. Mater. 24 (2014) 4935–4942.
[31] P. Wang, F. Casadei, S. Shan, J.C. Weaver, K. Bertoldi, Harnessing buckling to design tunable locally resonant acoustic metamaterials, Phys. Rev. Lett. 113 (2014), 014301.
[32] G.Y. Li, Y. Zheng, Y.P. Cao, X.Q. Feng, W.Y. Zhang, Controlling elastic wave propagation in a soft bilayer system via wrinkling-induced stress patterns, Soft Matter 12 (2016) 4204–4213.
[33] M. Kolle, A. Lethbridge, M. Kreysing, J.J. Baumberg, J. Aizenberg, P. Vukusic, Bio-inspired band-gap tunable elastic optical multilayer fibers, Adv. Mater. 25 (2013) 2239–2245.
[34] Y. Li, N. Kaynia, S. Rudykh, M.C. Boyce, Wrinkling of interfacial layers in stratified composites, Adv. Eng. Mater. 15 (2013) 921–926.
[35] S. Rudykh, C. Ortiz, M.C. Boyce, Flexibility and protection by design: imbricated hybrid microstructures of bio-inspired armor, Soft Matter 11 (2015) 2547–2554.
[36] K. Che, C. Yuan, J. Wu, H. Jerry Qi, J. Meaud, Three-dimensional-printed multistable mechanical metamaterials with a deterministic deformation sequence, J. Appl. Mech. 84 (2016), 011004.
[37] V. Slesarenko, N. Kazarinov, S. Rudykh, Distinct failure modes in bio-inspired 3D-printed staggered composites under non-aligned loadings, Smart Mater. Struct. 26 (2017) 035053.
[38] M.A. Biot, The influence of initial stress on elastic waves, J. Appl. Phys. 11 (1940) 522–530.
[39] P. Boulanger, M. Hayes, C. Trimarco, Finite-amplitude plane waves in deformed Hadamard elastic materials, Geophys. J. Int. 118 (1994) 447–458.
[40] P.C. Vinh, J. Merodio, On acoustoelasticity and the elastic constants of soft biological tissues, J. Mech. Mater. Struct. 8 (2013) 359–367.
[41] P.C. Vinh, J. Merodio, T.T.T. Hue, N.T. Nam, Non-principal Rayleigh waves in deformed transversely isotropic incompressible non-linearly elastic solids, IMA J. Appl. Math. 79 (2014) 915–928.
[42] N.T. Nam, J. Merodio, P.C. Vinh, The secular equation for non-principal Rayleigh waves in deformed incompressible doubly fiber-reinforced nonlinearly elastic solids, Int. J. Nonlin. Mech. 84 (2016) 23–30.
[43] S. Rytov, Acoustical properties of a thinly laminated medium, Sov. Phys. Acoust. 2 (1956) 68–80.
[44] D. Schneider, F. Liaqat, E.H. El Boudouti, Y. El Hassouani, B. Djafari-Rouhani, W. Tremel, H.J. Butt, G. Fytas, Engineering the hypersonic phononic band gap of hybrid bragg stacks, Nano Lett. 12 (2012) 3101–3108.
[45] K. Bertoldi, M.C. Boyce, Wave propagation and instabilities in monolithic and periodically structured elastomeric materials undergoing large deformations, Phys. Rev. B 78 (2008) 184107.
[46] V. Slesarenko, S. Rudykh, Microscopic and macroscopic instabilities in hyperelastic fiber composites, J. Mech. Phys. Solids 99 (2017) 471–482.
[47] P.I. Galich, V. Slesarenko, S. Rudykh, Shear wave propagation in finitely deformed 3D fiber-reinforced composites, Int. J. Solids Struct. 110–111 (110) (2017) 294–304.
[48] P. Zhang, W.J. Parnell, Soft phononic crystals with deformation-independent band gaps, Proc. R. Soc. A Math. Phys. Eng. Sci. 473 (2017) 20160865.